Journal of Nuclear Medicine, published on March 16, 2017 as doi:10.2967/jnumed.116.187161

11C-PBR28 or 18F-PBR111 detect white matter inflammatory heterogeneity in multiple sclerosis

Gourab Datta[1], Alessandro Colasanti[1, 2], Nicola Kalk[1], David Owen[1], Gregory Scott[1], Eugenii A. Rabiner[3], Roger N. Gunn[1, 3], Anne Lingford-Hughes[1], Omar Malik[1], Olga Ciccarelli[4], Richard Nicholas[1], Lei Nei[5], Marco Battaglini[6], Nicola D. Stefano[6], Paul M. Matthews[1]

[1]Division of Brain Sciences, Department of Medicine, Imperial College London, London, United Kingdom

[2]Centre for Affective Disorders, Psychological Medicine, Institute of Psychiatry, Psychology and Neuroscience, King's College London, London, United Kingdom

[3]Imanova Centre for Imaging Sciences, London, United Kingdom

[4] Queen Square Multiple Sclerosis Centre, Institute of Neurology, University College London, London, United Kingdom

[5]Department of Computing, Imperial College London, London, United Kingdom

[6]Department of Medicine, Surgery and Neurology, University of Siena, Siena, Italy

Running Title: TSPO PET in MS white matter and lesions

Word count: 5075 words

Address for correspondence:

Prof. Paul M. Matthews

p.matthews@imperial.ac.uk

E515, Division of Brain Sciences

Department of Medicine

Hammersmith Hospital

Du Cane Road, London WC12 0NN

Tel: +0044 207 594 2855

Address of first author:

Dr. Gourab Datta

gdatta1@ic.ac.uk

Postal address and phone as above

ABSTRACT

Objective: To assess microglial activation in lesions and in normal appearing white matter of multiple sclerosis (MS) patients using positron emission tomography (PET).

Methods: 34 MS patients (7 with secondary progressive MS (SPMS), 27 with relapsing remitting MS (RRMS)) and 30 healthy volunteers, genetically stratified for translocator protein (TSPO), binding status underwent PET scanning with TSPO radioligands (11C-PBR28 or 18F-PBR111). Regional TSPO availability was measured as a distribution volume ratio (DVR) relative to the caudate (a pseudo-reference region). White matter lesions (WML) were classified as "active" (DVR highest in the lesion), "peripherally active" (peri-lesional DVR highest), "inactive" (DVR highest in surrounding normal appearing white matter, NAWM) or "undifferentiated" (similar DVR across lesion, peri-lesional and NAWM volumes).

Results: The mean DVR in NAWM of patients was greater than that of the healthy volunteer white matter for both radioligands. Uptake for individual WML in patients was heterogeneous, but the median WML DVR and NAWM DVR for individual patients were strongly correlated ($\rho = 0.94$, $p= 4x10^{-11}$). A higher proportion of lesions were inactive in patients with SPMS (35 %) than RRMS (23 %), but active lesions were found in all patients, including those on highly efficacious treatments.

Conclusion: TSPO radioligand uptake was increased in brains of MS patients relative to healthy controls with two TSPO radiotracers. WML showed heterogeneous

patterns of uptake. Active lesions were found in patients with both RRMS and SPMS. Their independent prognostic significance needs further investigation.

Key Words: multiple sclerosis; white matter lesions; TSPO; PET; microglia

INTRODUCTION

MS is a chronic disease of the central nervous system characterised by multi-focal inflammatory demyelinating lesions. The number and distribution of the T2-hyperintense lesions (WML) in white matter found with magnetic resonance imaging (MRI) have a central role in the diagnosis of MS, but explain little of the future risk of disability progression (*1,2*).

The low predictive significance of WML may partially be explained by more diffuse inflammatory neuropathology evident in the white matter *post mortem* that appears normal on conventional MRI (*3*). Individual WML in the same brain and at different stages of disease also can have different neuropathological characteristics not well distinguished by MRI (*4*). Innate immune responses involving pro-inflammatory microglia are associated with both the focal and diffuse inflammation (*5-8*) .

The 18 kDa mitochondrial TSPO is highly expressed in activated microglia (*9*). Clinical studies using the first generation TSPO PET radioligand 11C-PK11195 reported higher global brain uptake in MS than healthy volunteers (*10*). WML showed variably increased or decreased TSPO radioligand uptake (*11,12*). Recent studies have highlighted more diffuse uptake (*13,14*). However, a challenge to interpretation of the literature overall is the use of different radioligands and different analytical methods.

In the present study, we have assessed *in vivo* PET TSPO radioligand binding in MS patients with 11C-PBR28 and re-analysed previously published data obtained with

18F-PBR111(*13*) and in healthy volunteers with 11C-PBR28 (*15-17*) using identical methodology. This allowed us to assess the consistency of results obtained with different radioligands and to compare characteristics of regional TSPO radioligand binding as an index of microglial/macrophage inflammatory activity in the MS NAWM and within WML. We explored whether individual lesions could be distinguished by patterns of TSPO ligand binding in analogous ways to histopathological classifications of lesions based on the distribution and abundance of activated microglia/macrophages (*18*).

MATERIALS AND METHODS

Subjects

The study protocol was approved by the West Bromley Research Ethics Committee (Ref No. 14/LO/0445). All subjects signed a written informed consent. MS was diagnosed according to the revised McDonald criteria (2010)(*19*). Subjects had a Expanded Disability Status Scale (EDSS) score $\leq$ 7.0 and none were treated with steroids or had a clinical relapse within 3 months of scanning. MS patients and healthy volunteers (HV) scanned with 18F-PBR111 and HV scanned with 11C-PBR28 were described previously (*13,15,17*).

TSPO Genotyping

TSPO genotype was assessed using a TaqMan based polymerase chain reaction (Applied Biosystems® QuantStudioTM 7) assay specific for the rs6971 polymorphism in the TSPO gene (*20*). Participants having genotypes associated with low affinity binding were excluded (*20,21*).

Imaging Methods

MRI Scanning

MRI scans were performed on a 3 Tesla Trio scanner (11C-PBR28 cohort) or a 3 Tesla Verio scanner (11C-PBR28 cohort) (both from Siemens Healthcare, Erlangen Germany). Volumetric T1-weighted images were acquired for all subjects using a 1 mm isotropic resolution, before and 5 minutes after intravenous gadolinium chelate (Dotarem®) administration. Volumetric T2-weighted images were acquired using a 1mm isotropic resolution.

MRI Image Processing and Definition of Regions of Interest

WML were segmented on the T2 image using Jim (Xinapse Systems version 7). The WML mask was used for lesion- filling the T1 image before segmentation into white matter, grey matter and cerebrospinal fluid using FMRIB Software Library tools (*22*). Peri-lesional masks were generated by dilating the WML mask in 3D by 6mm and subtracting the WML mask. A NAWM mask was created by subtracting the dilated WML mask from the total white matter mask and eroding by by 3mm. The Clinical

Imaging Centre Neuroanatomical Atlas was non-linearly deformed into each individual's T1 brain space for anatomical parcellations of regions of interest for PET analyses(*23*).

PET Scanning and Radioligand Synthesis

PET scanning (Discovery RX PET/CT scanner) was performed with a trans-axial resolution of 5.0 mm, and a radial resolution of 5.1 mm. 11C-PBR28 or [^{18}F]PBR111 were injected as an intravenous bolus over approximately 20 s at the start of a 90 min and 120 min dynamic PET acquisitions, respectively(*15,21*).
Radiosynthesis and quality control were performed on site also as previously described, with radiochemical purities of > 95% (*15,21*).

PET Image and Kinetic Analysis

T1 images, NAWM, WML, caudate and thalamus masks and reconstructed dynamic PET scans were used as inputs for the Molecular Imaging and Kinetic Analysis Toolbox software (*www.miakat.org*) for kinetic analysis of PET data. PET images were motion corrected using SPM5 (Wellcome Trust Centre for Neuroimaging, http://www.fil.ion.ucl.ac.uk/spm) for frame-by-frame rigid realignment .
Standardized uptake values (SUV) were calculated from the time-activity curves between 60 -90 minutes for 11C-PBR28 and 90-120 minutes for [^{18}F]PBR111 (*15,21*).

Transformed 4D PET images were integrated over time to obtain 3D PET summation images in Montreal Neurological Institute 2 mm space (*23*).

Reference based PET analyses enhances patient tolerance as arterial blood sampling is not needed. Here we used the Logan graphical reference method (*24*) to estimate regional brain DVR using the caudate time activity curve as the reference tissue input (*25*). Most previous MS studies also have used reference based methods (*10-12,14,26-28*). We and others have confirmed that reference based methods are strongly correlated with direct estimates of volume of distribution, V_T (*13,26,27,29*). While the reference tissue ideally is does not show specific (displaceable) ligand, TSPO which is expressed ubiquitously in the brain (*29*). Reference methods for TSPO have differed by the choice of reference tissue, broadly distinguished by those that use an individually variable reference, defined on the basis of appearing most similar to the behaviour expected for the healthy brain (*26,27*) and those that are anatomically defined and selected identical for all subjects (*12,28*). We chose to use the latter, as the interpretation and assumptions of lack of inter-patient heterogeneity are more directly tested.

All of these approaches technically define a "pseudo-reference" region and vary in dynamic range or sensitivity by the extent and variance in radioligand uptake in the region selected. We used the caudate nucleus because can be defined reliably using automated segmentation methods, show relatively lower levels of microglial activation in MS patients and TSPO binding relative to other brain regions (*21*). We

confirmed that there were no significant differences in the caudate SUV between people with MS and the HV for [^{18}F]PBR111 (mean ± s.d., 0.40 ± 0.11 for MS; 0.38 ± 0.07 for HV, p=0.67) and similarly for caudate SUV for [^{11}C]PBR28 (0.60 ± 0.14 for MS; 0.66 ± 0.13 for HV, p=0.26). We directly tested the accuracy of the relative uptakes estimated from the DVR calculated with the caudate "pseudo-reference" region and the ratio of SUV in brain regions to the SUV in caudate was strongly correlated with the DVR measure for MS and HV for both radioligands (Supplemental Fig. 1).

Individual Lesion Analysis and Classification

For the final analysis, WML with volume > 8 mm^3 were sampled to match the full-width half-maximum of the PET scanner of approximately 5 mm. Based on earlier results (*30*) and new test-retest PET data (Supplemental Fig. 2), four classes of lesions were identified based on the presence of differences in DVR > 5% in the lesion core and in the peri-lesional volume relative to surrounding NAWM: high uptake relative to surrounding NAWM ("active lesions"); highest uptake in the peri-lesional volume ("peripherally active lesions"); uptake similar to the NAWM ("undifferentiated lesions"); low uptake ("inactive lesions").

Statistical Analyses

Statistical analyses were performed using SPSS software (IBM, SPSS v22). The one-way analysis of variance was used to analyse the variance of between subjects factors. Homogeneity of variance was confirmed with Levene's test of equal variances. *Post hoc* analysis to assess differences between group means was performed with correction for multiple comparisons (Tukey's honest significant difference). Descriptive statistics were reported as mean ± standard deviation, unless otherwise stated. For correlational analyses, the Spearman's correlation coefficient was calculated, unless otherwise stated. A p-value (Bonferroni corrected for multiple comparsions) of less than 0.05 was considered statistically significant.

RESULTS

Demographic and clinical characteristics of study participants are summarised in Supplemental Tables 1 and 2. Data from 24 MS patients and 20 HV scanned with 11C-PBR28 and from 10 MS patients and 10 HV scanned with 18F-PBR111are included. The MS patients studied with the two radioligands were well matched for age, sex, EDSS and disease duration. However, approximately 30% of the 11C-PBR28 PET cohort had SPMS, while all of those in the 18F-PBR111PET group had RRMS.

Brain TSPO Radioligand Uptake

There were significant differences in the 11C-PBR28 DVR across brain regions for the MS and HV (one-way analysis of variance, $p=4x10^{-19}$). Uptake was highest in the thalamus; the thalamic 11C-PBR28 DVR in patients with MS (mean ± s.d., 1.52 ± 0.04)

was higher than in HV (1.39 ±0.05, p=0.03). The DVR of NAWM (1.17 ± 0.04) in the MS patients also was higher than in the white matter of HV (1.02 ± 0.05, p=0.02; Fig. 1A). 11C-PBR28 uptake in the NAWM was greater for patients than the mean uptake across WML (1.03 ± 0.04, p=0.03).

Our re-analysis of the smaller 18F-PBR111dataset found similar trends. Differences in DVR again were found between the MS and HV groups ($p=1x10^{-6}$). 18F-PBR111DVR in NAWM of the MS patients (1.27 ± 0.04) was greater than that in the HV white matter (1.13 ± 0.04, p=0.02; Fig. 1B) . The mean thalamic DVR for MS patients (1.50 ± 0.04) was greater than for HV (1.41 ± 0.04), although not statistically significantly so (p=0.08). We did not find differences between the mean DVR in the NAWM and WML (p=0.93).

Baseline disability (EDSS) was not correlated with DVR in any brain region studied for either radioligand.

TSPO Binding in NAWM and Individual WML of MS Patients

We evaluated differences in white matter DVR between subjects (Fig. 2). The ranges in DVR for 11C-PBR28 (median, 1.10, range 0.80-1.85, Supplemental Fig. 3) and for 18F-PBR111 (median 1.28, range 1.06 -1.45) amongst MS patients both were greater than for the white matter of HV (^{11}C-PBR28, median, 1.04, range, 0.82-1.21; 18F-PBR111, median 1.12, range, 0.98-1.25). Individual lesions in all subjects also

showed a wide variation in DVR (Fig. 2). There was a strong correlation between the median WML DVR and NAWM DVR (Spearman's ρ = 0.94 for both radioligands; p= $4x10^{-11}$ (11C-PBR28) or p= $1x10^{-4}$ (18F-PBR111)) (Fig. 3).

We found only two gadolinium enhancing lesions in scans from the MS patients. The gadolinium enhancing lesions (one in a patient scanned with 11C-PBR28 and one with 18F-PBR111) had high DVR (1.81 and 1.19, respectively), but not the highest DVR of lesions within those subjects (Fig. 2, A22 and B3).

Classification of Individual Lesions Based on Relative TSPO Uptake

We pooled data from the 11C-PBR28 and 18F-PBR111cohorts after classification of WML based on the magnitude and spatial distribution of the relative TSPO ligand uptake as active, inactive, peripherally active or undifferentiated (Methods and Fig. 4). A higher proportion of lesions were inactive in patients with SPMS (35 %, 39/112) than in those with RRMS (23 %, 103/446, p=0.01) (Fig. 5A). Inactive lesions were more common (31 %, 39/126) in patients with a longer disease duration than in those with shorter disease duration (18 %, 26/145; p=0.036) (Fig. 5B). However, active lesions were found in both clinical stages of disease (RRMS: 18 %, 82/446; SPMS: 28%, 31/112), across all quartiles of disease duration and in patients receiving any of the treatments represented in our population, as well as those not being treated (Fig. 5). 21 % (28/131) of sampled lesions in people being treated with nataluzimab (treated

between1-5.5 years) and 35 % (24/69) of the lesions in those who had received alemtuzimab were classified as active. Undifferentiated lesions were relatively most common in the patients with RRMS who were treatment naïve (70 %, 70/100).

DISCUSSION

We found similar relative differences between MS patients and HV using both TSPO PET radioligands. Both were associated with heterogeneity of TSPO tracer uptake in NAWM and between lesions in the MS patients. The strong correlation between the NAWM and WML TSPO uptake for individual patients suggests that these measures both reflect the same individually variable, innate inflammatory phenotype. The differences in inflammatory activity were not well reflected in the conventional MRI measures; gadolinium enhancement identified only two lesions out of a total of 558 lesions with increased TSPO radioligand uptake (Fig. 2). We found that lesions with diffusely high TSPO radioligand uptake (which we have called "active" lesions) can be found in all disease stages and treatment groups.

Although activated astrocytes can contribute to increased TSPO binding in some diseases, *post mortem* neuropathology suggests that activated microglia rather than astrocytes likely account for most TSPO binding in MS (*9*). The potential confound to quantitative estimation of the uptake of second generation TSPO ligands differences in second generation TSPO ligand affinity arising from the rs 6971 polymorphism can

be addressed by genetic stratification (*20*). Interpretation of differences in binding in terms of microglial activation in MS can thus be done with some confidence.

Neuropathology studies and *in vivo* PET TSPO imaging both provide evidence for a diffuse inflammatory process in white matter. This is associated with evidence of neuronal injury (*18,31,32*). Focal clusters or nodules of white matter microglial activation may precede the formation of WML (*33*). Consistent with these observations (and prior studies using 11C-PK11195), we found that TSPO binding was higher in the NAWM than in the white matter of HV (*11,12,14*). Increased uptake in the NAWM of patients with clinically isolated syndrome is associated with early development of clinically definite MS (*34*).

We found a heterogeneous pattern of microglial activation in WML relative to the NAWM both between and within MS patients. This heterogeneity is consistent with *post mortem* histopathology, which shows variable microglial activation between lesions (*6,35*). Prior studies also have shown variable TSPO radioligand uptake within lesions relative to NAWM (*11,12*). What has not been noted before is the strong correlation between the TSPO binding in NAWM and in WML. This suggests that patients are better described in terms of a global inflammatory state of their white matter rather than by individual lesion activity. Extending the earlier observations with clinically isolated syndrome (*34*), measures of this global white matter innate inflammatory activity may be predictive of the short term disease course generally for patients with MS.

We classified individual lesions into four different classes based on the patterns of TSPO radioligand uptake relative to that in the surrounding NAWM. The classification is similar conceptually to that used histopathologically for WML in MS brains: both rely on differences in distributions of activated microglia (*35*). In our study, we identified all four of these lesion types *in vivo* in all disease stages. There were a higher proportion of inactive lesions in patients with longer disease duration and with SPMS than in RRMS. These findings *in vivo* are reflected in a recent study of brains *post mortem,* where histopathologically defined inactive lesions are more common with SPMS and longer disease duration (*5*). However, we also found that TSPO PET "active" lesions were more common in brains of patients with SPMS than those from patients with RRMS. Unexpectedly, we found active lesions even in patients receiving either of two of the most efficacious pharmacological immunomodulators (alemtuzimab and nataluzimab).

These data thus provide further evidence for substantial persistent innate inflammatory activity in SPMS (*10*). They also suggest that current treatments classed as highly efficacious based on suppression of T2 hyperintense lesion activity do not suppress microglial activity fully. Persistent, pro-inflammatory microglia could explain the progression of neurodegenerative changes reflected as brain atrophy or disability progression that are seen in some patients(*35*). However, alternative microglial activation phenotypes also can contribute to reparative processes(*36*).

Baseline T2 lesion load and clinical progression are weakly correlated (*37*). Previous TSPO PET studies have reported positive correlations between disability (EDSS) and TSPO ligand uptake (*10,13*), but we did not observe this with either of our two patient groups. This may be related to sample sizes, as neither study was powered for this outcome. The lack of correlation between disability and TSPO uptake could reflect limitations of a cross-section design: disability measures reflect the summary impact of relevant injury to date, whereas the PET measures are determined by inflammatory activity only at the time of the scan. Insensitivity of EDSS to all relevant dimensions of disability could also contribute (*38*). Finally, quantifying TSPO binding using a pseudo-reference region method may have led to an underestimation of regional radioligand uptake (35). The reduced dynamic range of the reference-based measure could limit discrimination of differences between tissues, despite the gain in precision. We also did not have repeat examinations on all subjects, so we had to define meaningful differences in DVR based on a "hard threshold" estimated from independent test-retest estimates.

In vitro, *ex vivo* and *in silico* data indicate that 11C-PBR28 has higher binding affinity for TSPO and higher displaceable to nondisplaceable binding compared with 18F-PBR111, when matched for TSPO binding status (*39*). A study using a TSPO agonist (XBD173) to block binding of 11C-PBR28 in healthy volunteers directly confirmed estimates of relatively high displaceable (specific) binding for this ligand (*15*). The dynamic range of DVR in the MS patients measured with 11C-PBR28 was

greater than with 18F-PBR111. Finally, defluorination of the 18F-PBR111 and skull uptake of 18F (*40*) limits accuracy of assessment of uptake in the adjacent neocortex. Together, these factors suggest that for many applications, 11C-PBR28 is a preferable radioligand. However, the longer half-life of 18F-PBR111 (110 minutes) than 11C-PBR28 (20 minutes) makes the former more practical for transportation between sites without the need for having an on site cyclotron to produce the radioligand. Further work needs to be done, for instance with blocking studies of 18F-PBR111, to characterise the *in vivo* binding characteristics of both radioligands, but, depending on manufacturer/supply arrangements, 18F-PBR111 could have advantages at some sites.

CONCLUSION

Our report provides further evidence for continuing inflammation and heterogeneity in the innate immune inflammatory activity of individual lesions and NAWM of patients with MS that is not captured by conventional MRI. Our results highlight that gadolinium contrast enhancement underestimates the total inflammatory activity. We also found that the overall innate inflammatory activity was not appreciably lower in patients with RRMS relative to SPMS. We hypothesise that this inflammation contributes to determining the prognosis of individual patients. PET may provide a pharmacodynamic marker for treatments targeting this

activity. Longitudinal studies now are needed to establish the clinical significance of these and related observations from other laboratories.

DISCLOSURES

PMM, ALH, AC, NK, GD received support from grants from GSK during the conduct of these studies. EAR and PMM are past employees and current shareholders in GSK. None of the other co-authors has a financial or other conflict of interest.

ACKNOWLEDGEMENTS

GD is grateful for support as a fellow through the Imperial Wellcome Trust-GlaxoSmithKline Clinical Fellowship Training Scheme. This article presents independent research funded by this fellowship scheme and supported by the NIHR CRF at Imperial College Healthcare NHS Trust. PMM acknowledges generous support from Edmond J Safra Foundation and Lily Safra and research funding through the Imperial Biomedical Research Centre and the NIHR Investigator programme.

REFERENCES

1. Bar-Zohar D, Agosta F, Goldstaub D, Filippi M. Magnetic resonance imaging metrics and their correlation with clinical outcomes in multiple sclerosis: a review of the literature and future perspectives. *Mult Scler.* 2008;14:719-727.

2. Goodin DS. Magnetic resonance imaging as a surrogate outcome measure of disability in multiple sclerosis: have we been overly harsh in our assessment? *Ann Neurol.* 2006;59:597-605.

3. Allen IV, McQuaid S, Mirakhur M, Nevin G. Pathological abnormalities in the normal-appearing white matter in multiple sclerosis. *Neurol Sci.* 2001;22:141-144.

4. Filippi M, Rocca MA, Barkhof F, et al. Association between pathological and MRI findings in multiple sclerosis. *Lancet Neurol.* 2012;11:349-360.

5. Frischer JM, Weigand SD, Guo Y, et al. Clinical and pathological insights into the dynamic nature of the white matter multiple sclerosis plaque. *Ann Neurol.* 2015;78:710-721.

6. Frischer JM, Bramow S, Dal-Bianco A, et al. The relation between inflammation and neurodegeneration in multiple sclerosis brains. *Brain.* 2009;132:1175-1189.

7. Mahad DH, Trapp BD, Lassmann H. Pathological mechanisms in progressive multiple sclerosis. *Lancet Neurol.* 2015;14:183-193.

8. Kutzelnigg A, Lucchinetti CF, Stadelmann C, et al. Cortical demyelination and diffuse white matter injury in multiple sclerosis. *Brain.* 2005;128:2705-2712.

9. Cosenza-Nashat M, Zhao ML, Suh HS, et al. Expression of the translocator protein of 18 kDa by microglia, macrophages and astrocytes based on immunohistochemical localization in abnormal human brain. *Neuropathol Appl Neurobiol.* 2009;35:306-328.

10. Politis M, Giannetti P, Su P, et al. Increased PK11195 PET binding in the cortex of patients with MS correlates with disability. *Neurology.* 2012;79:523-530.

11. Banati RB, Newcombe J, Gunn RN, et al. The peripheral benzodiazepine binding site in the brain in multiple sclerosis: quantitative in vivo imaging of microglia as a measure of disease activity. *Brain.* 2000;123 (Pt 11):2321-2337.

12. Debruyne JC, Versijpt J, Van Laere KJ, et al. PET visualization of microglia in multiple sclerosis patients using [11C]PK11195. *Eur J Neurol.* 2003;10:257-264.

13. Colasanti A, Guo Q, Muhlert N, et al. In Vivo Assessment of Brain White Matter Inflammation in Multiple Sclerosis with (18)F-PBR111 PET. *J Nucl Med.* 2014;55:1112-1118.

14. Rissanen E, Tuisku J, Rokka J, et al. In Vivo Detection of Diffuse Inflammation in Secondary Progressive Multiple Sclerosis Using PET Imaging and the Radioligand (1)(1)C-PK11195. *J Nucl Med.* 2014;55:939-944.

15. Owen DR, Guo Q, Kalk NJ, et al. Determination of [(11)C]PBR28 binding potential in vivo: a first human TSPO blocking study. *J Cereb Blood Flow Metab.* 2014;34:989-994.

16. Vera JH, Guo Q, Cole JH, et al. Neuroinflammation in treated HIV-positive individuals: A TSPO PET study. *Neurology.* 2016.

17. Guo Q, Owen DR, Rabiner EA, Turkheimer FE, Gunn RN. A graphical method to compare the in vivo binding potential of PET radioligands in the absence of a reference region: application to [(1)(1)C]PBR28 and [(1)(8)F]PBR111 for TSPO imaging. *J Cereb Blood Flow Metab.* 2014;34:1162-1168.

18. Lassmann H, Bruck W, Lucchinetti CF. The immunopathology of multiple sclerosis: an overview. *Brain Pathol.* 2007;17:210-218.

19. Polman CH, Reingold SC, Banwell B, et al. Diagnostic criteria for multiple sclerosis: 2010 revisions to the McDonald criteria. *Ann Neurol.* 2011;69:292-302.

20. Owen DR, Yeo AJ, Gunn RN, et al. An 18-kDa translocator protein (TSPO) polymorphism explains differences in binding affinity of the PET radioligand PBR28. *J Cereb Blood Flow Metab.* 2012;32:1-5.

21. Guo Q, Colasanti A, Owen DR, et al. Quantification of the specific translocator protein signal of 18F-PBR111 in healthy humans: a genetic polymorphism effect on in vivo binding. *J Nucl Med.* 2013;54:1915-1923.

22. Battaglini M, Jenkinson M, De Stefano N. Evaluating and reducing the impact of white matter lesions on brain volume measurements. *Hum Brain Mapp.* 2012;33:2062-2071.

23. Tziortzi AC, Searle GE, Tzimopoulou S, et al. Imaging dopamine receptors in humans with [11C]-(+)-PHNO: dissection of D3 signal and anatomy. *Neuroimage.* 2011;54:264-277.

24. Logan J, Fowler JS, Volkow ND, Wang GJ, Ding YS, Alexoff DL. Distribution volume ratios without blood sampling from graphical analysis of PET data. *J Cereb Blood Flow Metab.* 1996;16:834-840.

25. Gunn RN, Gunn SR, Cunningham VJ. Positron emission tomography compartmental models. *J Cereb Blood Flow Metab.* 2001;21:635-652.

26. Turkheimer FE, Edison P, Pavese N, et al. Reference and target region modeling of [11C]-(R)-PK11195 brain studies. *J Nucl Med.* 2007;48:158-167.

27. Herranz E, Gianni C, Louapre C, et al. Neuroinflammatory component of gray matter pathology in multiple sclerosis. *Ann Neurol.* 2016;80:776-790.

28. Colasanti A, Guo Q, Giannetti P, et al. Hippocampal Neuroinflammation, Functional Connectivity, and Depressive Symptoms in Multiple Sclerosis. *Biol Psychiatry.* 2016;80:62-72.

29. Kropholler MA, Boellaard R, Schuitemaker A, Folkersma H, van Berckel BN, Lammertsma AA. Evaluation of reference tissue models for the analysis of [11C](R)-PK11195 studies. *J Cereb Blood Flow Metab.* 2006;26:1431-1441.

30. Coughlin JM, Wang Y, Ma S, et al. Regional brain distribution of translocator protein using [(11)C]DPA-713 PET in individuals infected with HIV. *J Neurovirol.* 2014;20:219-232.

31. Geurts JJ, Bo L, Roosendaal SD, et al. Extensive hippocampal demyelination in multiple sclerosis. *J Neuropathol Exp Neurol.* 2007;66:819-827.

32. Lassmann H, van Horssen J, Mahad D. Progressive multiple sclerosis: pathology and pathogenesis. *Nat Rev Neurol.* 2012;8:647-656.

33. Singh S, Metz I, Amor S, van der Valk P, Stadelmann C, Bruck W. Microglial nodules in early multiple sclerosis white matter are associated with degenerating axons. *Acta Neuropathol.* 2013;125:595-608.

34. Giannetti P, Politis M, Su P, et al. Increased PK11195-PET binding in normal-appearing white matter in clinically isolated syndrome. *Brain.* 2015;138:110-119.

35. Lucchinetti C, Bruck W, Parisi J, Scheithauer B, Rodriguez M, Lassmann H. Heterogeneity of multiple sclerosis lesions: implications for the pathogenesis of demyelination. *Ann Neurol.* 2000;47:707-717.

36. Ransohoff RM. A polarizing question: do M1 and M2 microglia exist? *Nat Neurosci.* 2016;19:987-991.

37. Sormani MP, Arnold DL, De Stefano N. Treatment effect on brain atrophy correlates with treatment effect on disability in multiple sclerosis. *Ann Neurol.* 2014;75:43-49.

38. Stangel M, Penner IK, Kallmann BA, Lukas C, Kieseier BC. Towards the implementation of 'no evidence of disease activity' in multiple sclerosis treatment: the multiple sclerosis decision model. *Ther Adv Neurol Disord.* 2015;8:3-13.

39. Guo Q, Owen DR, Rabiner EA, Turkheimer FE, Gunn RN. Identifying improved TSPO PET imaging probes through biomathematics: the impact of multiple TSPO binding sites in vivo. *Neuroimage.* 2012;60:902-910.

40. Fookes CJ, Pham TQ, Mattner F, et al. Synthesis and biological evaluation of substituted [18F]imidazo[1,2-a]pyridines and [18F]pyrazolo[1,5-a]pyrimidines for the study of the peripheral benzodiazepine receptor using positron emission tomography. *J Med Chem.* 2008;51:3700-3712.

Figure Legends

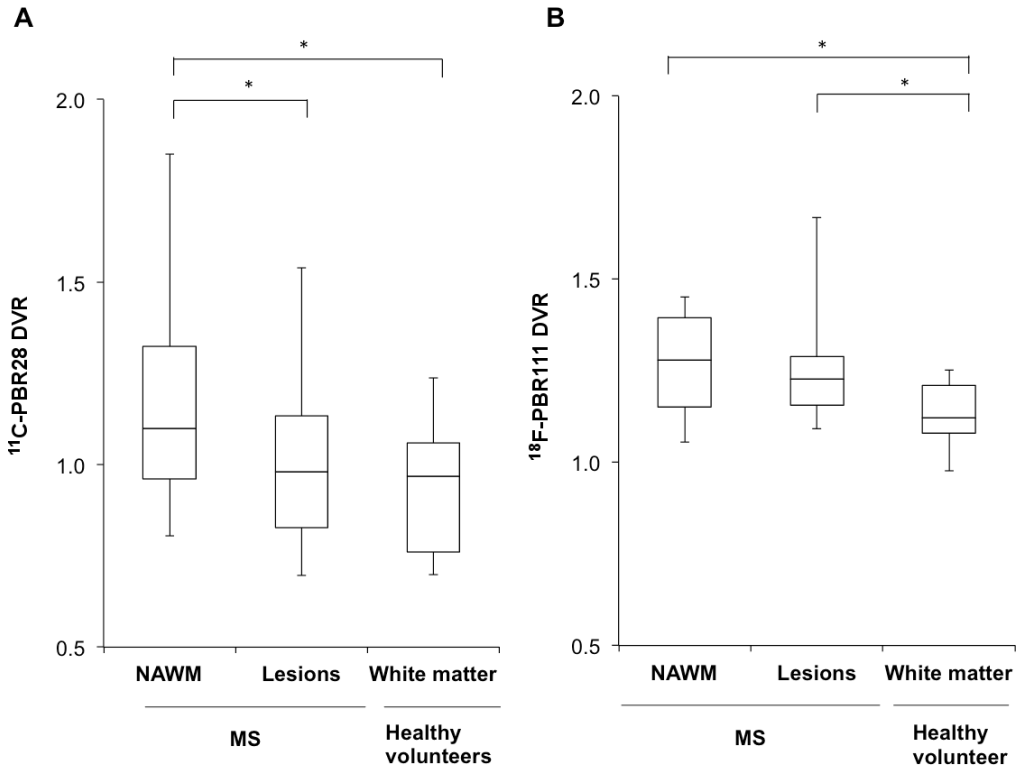

FIGURE 1. Boxplots of the distribution volume ratio (DVR) in white matter of healthy volunteers and normal appearing white matter (NAWM) and lesions in multiple sclerosis (MS) using (A) 11C-PBR28 and (B) 18F-PBR111. *p<0.05 was considered a statistically significant different DVR between brain regions.

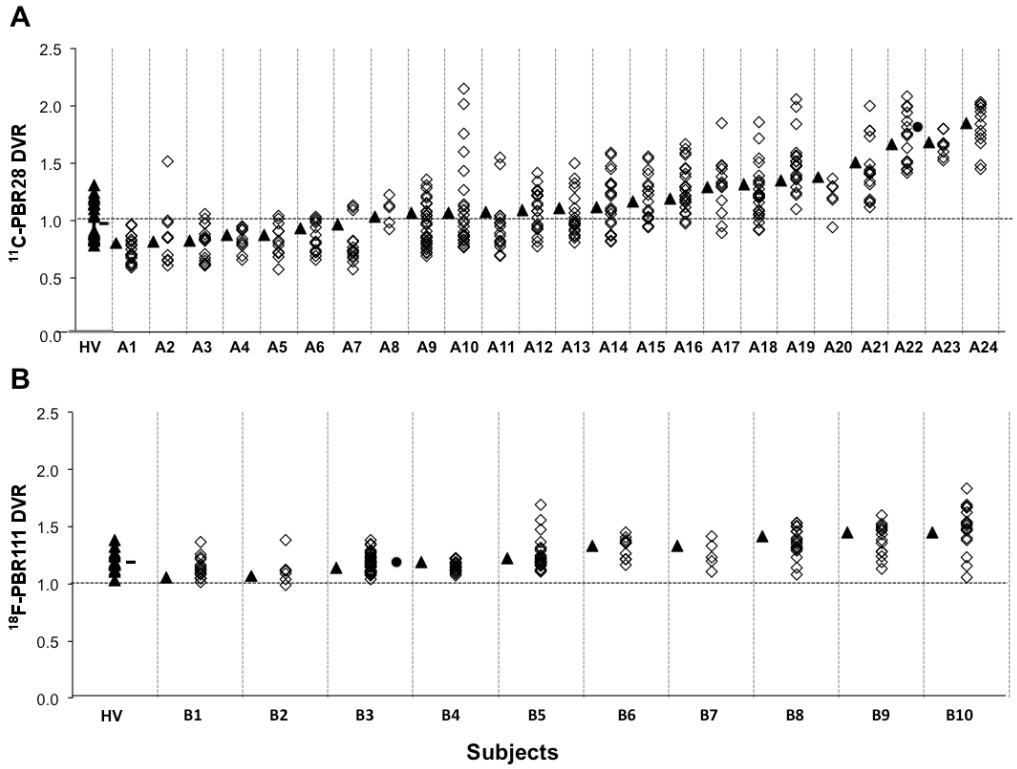

FIGURE 2. PET distribution volume ratios (DVR) determined for (A) 11C-PBR28 and (B) 18F-PBR111 in the white matter of individual healthy volunteers (filled black triangles) and in normal appearing white matter (NAWM, filled black triangles) and in individual white matter lesions (open diamonds; median, horizontal black bar), including gadolinium enhancing lesions (filled black circles) of MS patients. Data from all healthy volunteers (HV) are shown in a single bar on the far left side. Data from individual MS patients (rank ordered with respect to the NAWM DVR) are shown to the right. A1- A24 and B1-B10 denote individual MS patients scanned with 11C-PBR28 and 18F-PBR111, respectively. Detailed demographic information is provided in Supplementary Table 2.

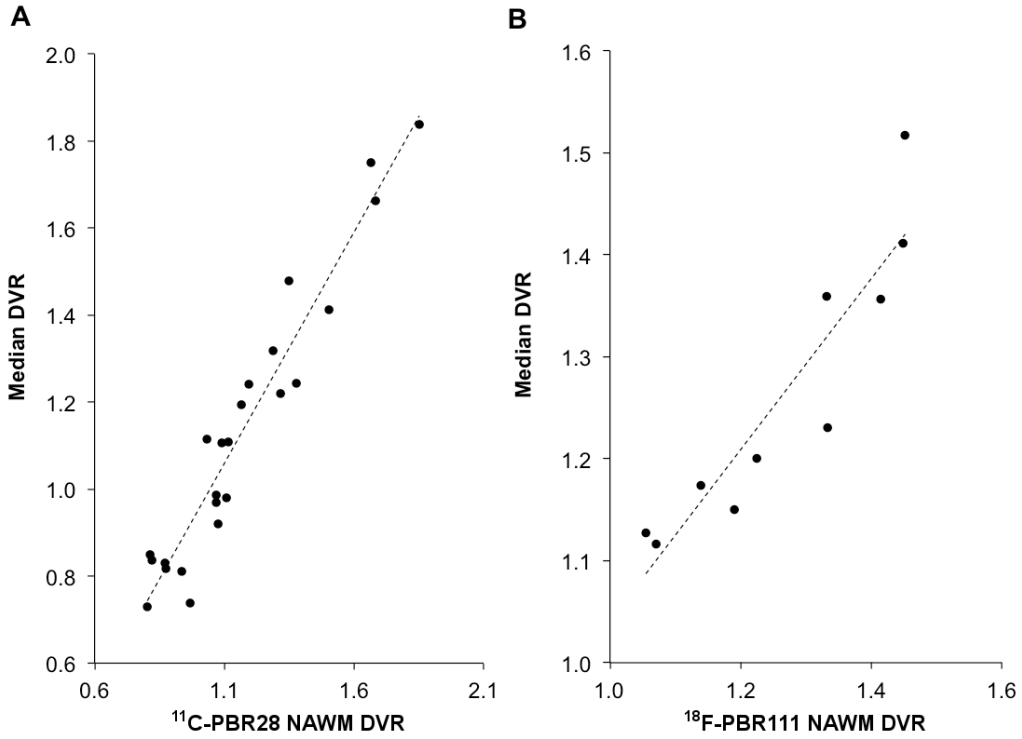

FIGURE 3. Strong positive correlations between median PET distribution volume ratios (DVR) were found using both (A) 11C-PBR28 (Spearman's $\rho = 0.94$, $p = 4x10^{-11}$) and (B) 18F-PBR111 ($\rho = 0.94$, $p = 1x10^{-4}$) between DVR in white matter lesions (ordinate) and in the normal appearing white matter (NAWM) (abscissa) for MS patients.

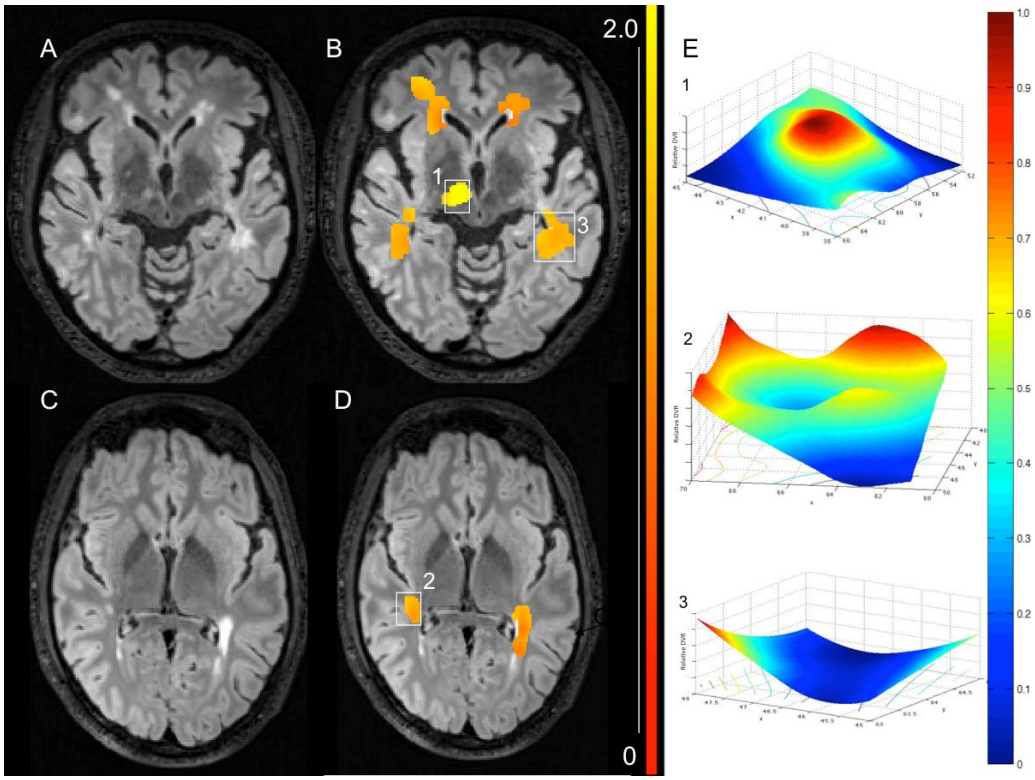

FIGURE 4. Axial T2 FLAIR images (A-D) from two MS patients (participants A20 [A, B] and A10 [C, D], respectively) with corresponding overlays of parametric 11C-PBR28 PET distribution volume ratios (DVR) within and around larger white matter T2 hyperintense lesions (B, D). To their right is a colour scale for DVR values. (E) Includes surface renderings of relative DVR variation across voxels for lesions identified as to the left as 1-3 (B, D). To discriminate voxel-wise variation more clearly, DVR has been transformed by a non-linear scaling function, with relative values expressed as shown on the colour scale to the right and as relative excursion above the origin. The base of the plot has axes ordered by voxels in the image plane (x, y). Three lesion types are illustrated: (1) an active lesion; (2) a peripherally active lesion; and (3) an 'undifferentiated' lesion.

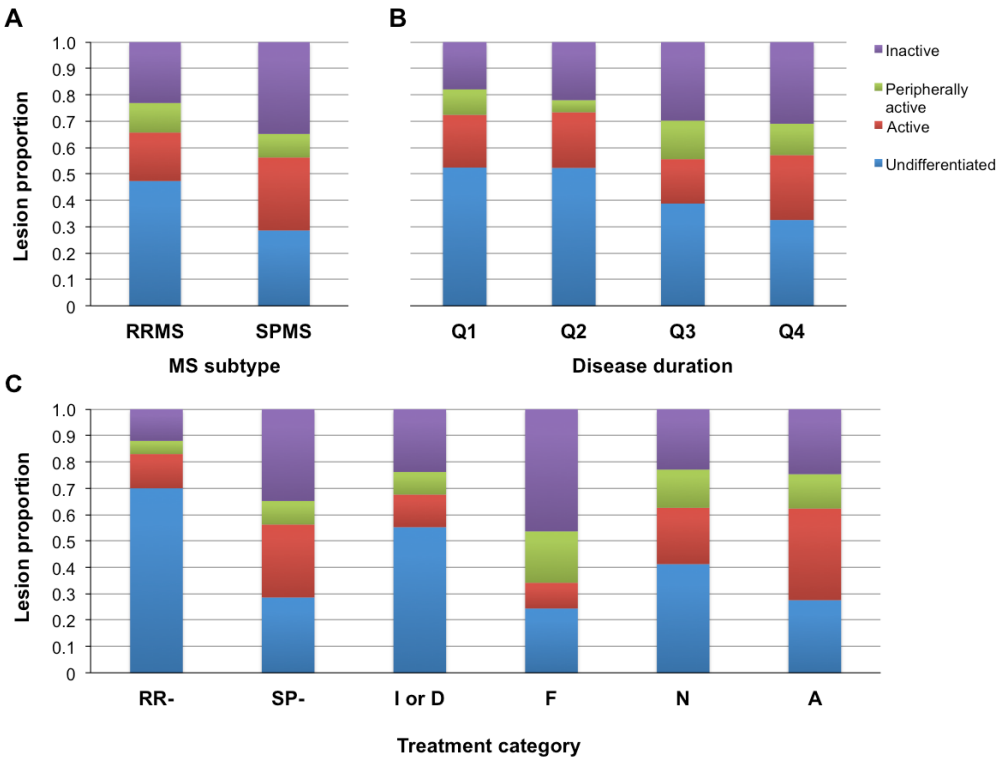

FIGURE 5. Proportions of the four types of white matter lesions) characterised by PET in MS patients. Data from subjects studied with 11C-PBR28 and 18F-PBR111 have been combined. Plots illustrate relative abundance of lesions classified by: (A) clinical MS subtype (relapsing remitting, RR: secondary progressive, SP) and (B) disease duration of subjects (expressed as quartiles (Q) across the study population: Q1, 1-7 years; Q2, 8-11 years; Q3, 12-16 years; Q4, 17-28 years). (C) Relative proportion of lesions group according to treatment at the time of scanning: no treatment in people with relapsing remitting (RR-) or secondary progressive (SP-); disease modifying treatment with interferon or dimethyl fumarate (I or D); fingolimod (F); nataluzimab (N) and alemtuzimab (A).

SUPPLEMENTARY MATERIALS

SUPPLEMENTAL FIGURE LEGENDS

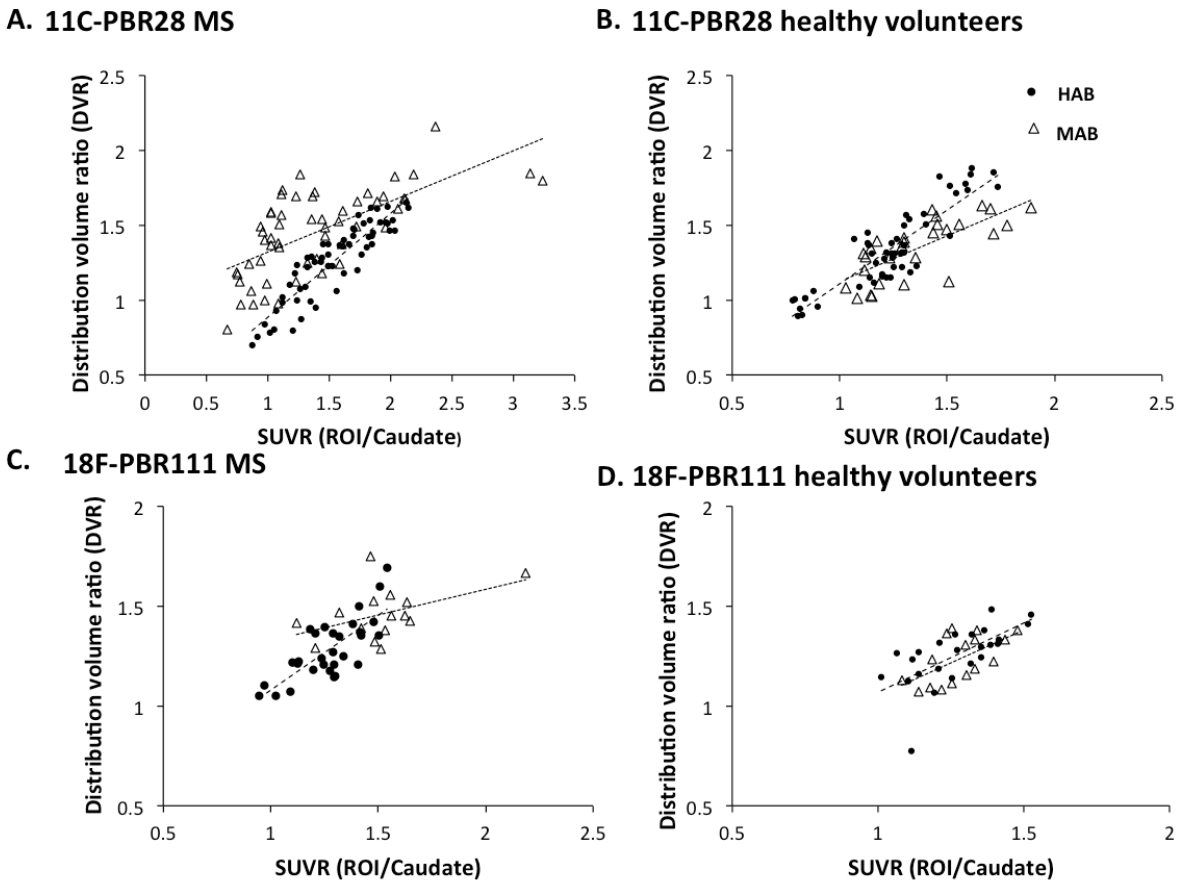

SUPPLEMENTAL FIGURE 1. Plots of distribution volume ratio (DVR) using the Logan method with a caudate pseudo-reference region against standarized uptake value ratio (SUV) as a ratio of the SUV in caudate (SUVR) for both 11C-PBR28 (SUV between 60 to 90 minutes) and 18F-PBR111 (SUV between 90 to 120 minutes) for high affinty binders (HAB) and medium affinity binders (MAB) for translocator protein (TSPO) across all brain regions of interest (ROI) analysed (thalamus, cerebellum, cortex, white matter, normal appearing white matter and white matter lesions). Regression lines are plotted separately for HAB (dashed line) and MAB (dotted line). Separate plots were made for (A) 11C-PBR28

multiple sclerosis (MS) patients (regression line gradient for HAB is 0.69, for MAB is 0.34), (B) 11C-PBR28 healthy volunteers (regression line gradient for HAB is 0.99, for MAB is 0.61), (C) 18F-PBR111 MS patients (regression line gradient for HAB is 0.75, for MAB is 0.26) and (D) 18F-PBR111 healthy volunteers (regression line gradient for HAB is 0.70, for MAB is 0.66). Each data point represents a single brain region from an individual subject. These figures indicates that raw SUVR measures are correlated with DVR using a caudate pseudoreference region for all brain regions studied, both tracers and both MS and healthy volunteers, discussed in detail here in the Supplementary Methods.

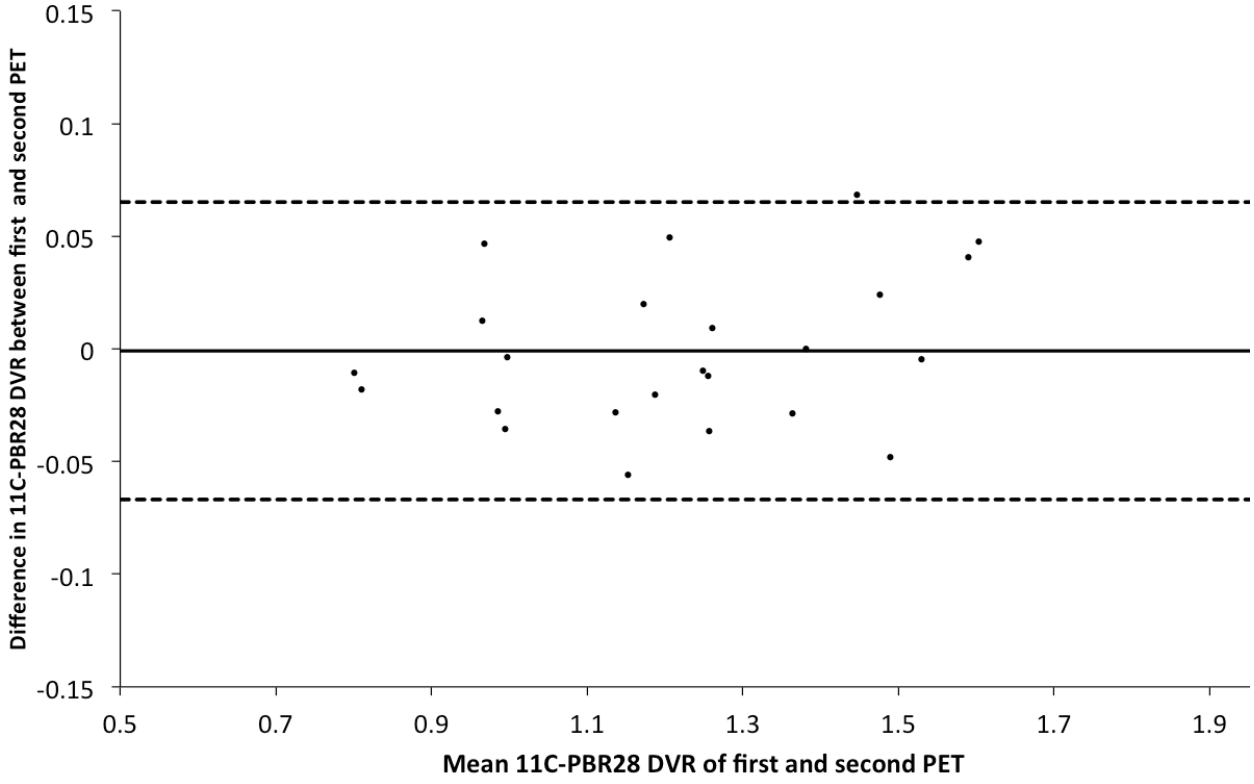

SUPPLEMENTAL FIGURE 2. Bland-Altman plot for six MS patients who had two 11C-PBR28 PET scans within six weeks of each other with no clinical changes in that period for three brain regions (white matter lesions, normal appearing white matter, thalamus and cortex). Each data point represents a single brain region from one patient (n=24). The test-retest variability of DVR between the first PET scan ("test") and second scan ("retest") was calculated for each datapoint as ordinate value divided by abscissa value. The mean test-retest variability in DVR between the two PET scans was 2.26 % (standard deviation +/- 1.45 %). The DVR test-retest variability for all regions and patients was < 5 %. The unbroken line intersects the vertical axis at the mean test-retest difference in DVR; the upper and lower dotted lines intersect the vertical axis at the mean ± 1.96 standard deviations of the test-retest difference in DVR.

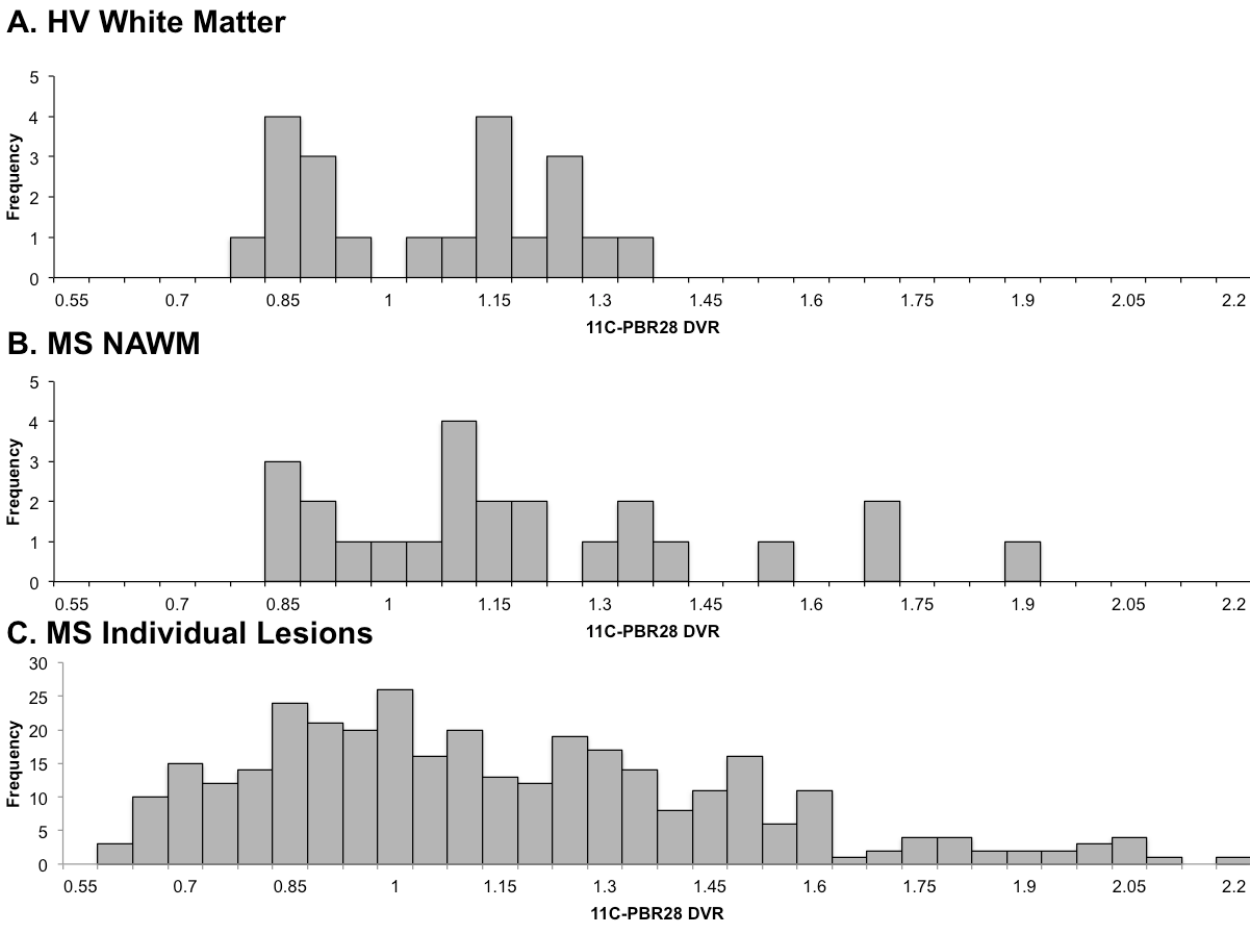

SUPPLEMENTAL FIGURE 3. Histograms showing the frequency distributions of 11C-PBR28 distribution volume ratio (DVR) in (A) white matter of healthy volunteers (HV), (B) normal appearing white matter (NAWM) of MS patients and (C) individual white matter lesions collated across all the MS patients in the 11C-PBR28 cohort.

SUPPLEMENTAL TABLES

Demographic/clinical characteristic	18F-PBR111 HV[1]	11C-PBR28 HV[2]	18F-PBR111 MS[1]	11C-PBR28 MS[3]
Number	10	20	10	24
Gender, Male : Female, n	3 : 7	14 : 6	2 : 8	10 : 14
Age, years, mean (SD)	42(11.1)	47 (14.8)	45 (8.8)	47 (11.4)
TSPO genotype, n				
High affinity binders	7	12	7	13
Medium affinity binders	3	8	3	11
MS subtype, RRMS: SPMS, n			10 : 0	17 : 7
Disease duration, years, mean (SD)			10 (5.8)	13.5 (6.5)
EDSS, median (range)			3.5 (1.5-6.5)	4.5 (1.0-7.0)
Treatments, n				
None			3	9
Interferons			5	1
Fingolimod			0	3
Dimethyl fumarate			2	1
Nataluzimab			0	6
Alemtuzimab			0	4
MRI metrics (normalised)				
Brain parenchymal volume(cm^3), mean (SD)	1534 (58)	1590(180)	1440 (126)	1380 (140)
Cortical volume(cm^3), mean (SD)	637 (33)	630 (55)	616 (61)	578 (66)
Mean T2 white matter lesion volume (cm^3) (SD)			9.7 (9.7)	17.9 (15.8)
Median T2 white matter lesion number (range)			31.5 (7-52)	38.5 (13-96)

Supplemental Table 1. Demographic characteristics of healthy volunteers (HV) and MS patients scanned with either 11C-PBR28 or 18F-PBR111

Abbreviations: MS=multiple sclerosis; RRMS=relapsing remitting MS; SPMS=secondary progressive MS; TSPO=translocator protein; EDSS=Expanded Disability Status Scale; SD=standard deviation

Data from subjects previously described in:
[1] Colasanti et al. 2014 (*1*)
[2] Owen et al. 2014; Guo et al. 2014; Vera et al. 2016 (*2-4*)
[3] Datta et al. 2016 (*5*)

Case	Age	Gender	EDSS	Disease duration	MSSS	MS Subtype	DMT
A1	22	F	3	16	2.6	RRMS	Fingolimod
A2	38	M	6	10	7.4	RRMS	Alemtuzimab
A3	42	F	1	13	0.6	RRMS	Nataluzimab
A4	50	F	2.5	9	3.5	RRMS	-
A5	59	M	6	23	5.2	SPMS	-
A6	36	M	1	6	1.1	RRMS	Dimethyl fumarate
A7	57	F	1	18	0.3	RRMS	Fingolimod
A8	48	M	7	12	8.6	RRMS	Nataluzimab
A9	53	M	5	14	5.2	RRMS	Nataluzimab
A10	43	M	5	13	5.3	SPMS	-
A11	29	F	1	1	2.4	RRMS	Interferon β
A12	51	F	6.5	8	8.7	RRMS	Nataluzimab
A13	62	F	6	24	5.0	SPMS	-
A14	56	M	7	17	7.8	SPMS	-
A15	52	F	2	6	3.5	RRMS	Alemtuzimab
A16	45	F	4	28	2.4	RRMS	Alemtuzimab
A17	66	F	6.5	17	6.9	RRMS	-
A18	53	F	3	16	2.6	RRMS	-
A19	30	F	4	6	6.8	RRMS	Nataluzimab
A20	36	M	7	10	8.9	SP	-
A21	47	M	7	11	8.8	SPMS	-
A22	39	M	4	10	5.3	RRMS	Alemtuzimab
A23	45	F	6.5	14	7.6	RRMS	Fingolimod
A24	64	F	2.5	22	1.3	RRMS	Nataluzimab
B1	42	F	6	2	9.6	RRMS	Interferon β
B2	40	F	4	11	4.9	RRMS	Natalizumab
B3	41	F	1.5	14	2.3	RRMS	-
B4	51	F	2	4	8.6	RRMS	Interferon β
B5	28	M	2	7	3.2	RRMS	-
B6	55	F	2	20	0.9	RRMS	Interferon β
B7	42	M	5.5	11	6.3	RRMS	-
B8	48	F	6.5	8	8.71	RRMS	Natalizumab
B9	59	F	3	16	2.6	RRMS	Interferon β
B10	41	F	5.5	4	9.1	RRMS	Interferon β

Supplemental Table 2. Demographic and clinical characteristics of individual MS patients. A1-24: 11C-PBR28 cohort (data from these patients was used in Datta et al. 2016(*5*)); B1-10:18F-PBR111 cohort (data from these patients was published with a different analysis in Colasanti et al.

2014(*1*))Abbreviations: MS=multiple sclerosis; M=male; F=female; EDSS=Expanded Disability Status Scale; RRMS=relapsing remitting multiple sclerosis; SPMS=secondary progressive multiple sclerosis

REFERENCES

1. Colasanti A, Guo Q, Muhlert N, et al. In vivo sssessment of brain white matter inflammation in multiple sclerosis with (18)F-PBR111 PET. *J Nucl Med.* 2014;55:1112-1118.

2. Guo Q, Owen DR, Rabiner EA, Turkheimer FE, Gunn RN. A graphical method to compare the in vivo binding potential of PET radioligands in the absence of a reference region: application to [(1)(1)C]PBR28 and [(1)(8)F]PBR111 for TSPO imaging. *J Cereb Blood Flow Metab.* 2014;34:1162-1168.

3. Owen DR, Guo Q, Kalk NJ, et al. Determination of [(11)C]PBR28 binding potential in vivo: a first human TSPO blocking study. *J Cereb Blood Flow Metab.* 2014;34:989-994.

4. Vera JH, Guo Q, Cole JH, et al. Neuroinflammation in treated HIV-positive individuals: a TSPO PET study. *Neurology.* 2016;86:1425-1432.

5. Datta G, Violante IR, Scott G, et al. Translocator positron-emission tomography and magnetic resonance spectroscopic imaging of brain glial cell activation in multiple sclerosis. *Mult Scler.* 2016;0: 1-10.